



Electronics and Optical Properties of Nitrogen Doped Anatase for Solar Application

Olayinka A. S.^{1,*}, Nwankwo W.² & Idiodi J. O. A.³

¹Department of Physics, Edo University Iyamho, Edo State, Nigeria.

²Department of Computer Science, Edo University Iyamho, Edo State, Nigeria.

³Department of Physics, University of Benin, Benin city, Nigeria.

*akinola.olayinka@edouniversity.edu.ng; solayinkaa@gmail.com

Received: xxxx xxxxxx, 2019 Accepted: xxxx xxxxxx, 2019

Date of Publication: December, 2019

Abstract: One of the major problems in developing countries is dearth of sufficient energy, which in turn hampers sustainable development. Anatase is one of the prominent polymorph of Titanium dioxide (TiO₂) with great potential for solar application except for its wide band gap which limits its solar energy utilization to about 4%. It has fascinated much devotion from researchers owing to its extensive array of applications coupled with its availability and cost effectiveness. Doping has been presented as a means to narrow the band gap thereby enhancing its efficiency for solar application. Electronic and optical properties are presented here for pure and Nitrogen (N) doped anatase. The study is based on the density functional theory (DFT) using generalized gradient approximation (GGA) in addition to Coulomb Interaction (U) as implemented in quantum espresso code while the optical properties calculation was done with the Yambo code. With the inclusion of U parameter of 12.5eV, band gap of 3.1eV was obtained which compared favorably with experimental results. Doping concentration of 3.1% gave rise to band narrowing while Partial density of state (PDOS) shows that the band narrowing in anatase is due to the contribution from 2p state of the Nitrogen dopant. The optical properties calculated revealed that N-doped anatase has optical crests in the visible light range of electromagnetic spectrum which makes it a potential material for solar application with higher efficiency than pure anatase.

Keyword: Anatase, doping, solar, dielectric constant.

Introduction

Recently, South Africa commissioned her first solar powered airport which happened to be the first in Africa after the first was launched in India few years ago. The airport generates 750 kW every day against 400kW required to run it daily[1]. African especially Nigeria is favoured in term of daily solar radiation of up to 220 W/m^2 as against about 150 W/m^2 for USA and 100 W/m^2 for Europe [2], thereby making it a stanch source of energy that is also renewable. Solar radiation is freely available; however, the major setback is the high cost associated with solar panels, making it inaccessible to the majority of growing populace in dare need of power to foster and drive sustainable developments. Anatase is a Polymorph of titanium dioxide (TiO_2) and it is a wide band gap material. TiO_2 is nontoxic and relatively inexpensive. It is physically and chemically stable [3-5]. TiO_2 is useful as photo-catalyst in solar applications, electric gas sensor, white pigments, biomaterials, memory devices and optical coatings [6-9]. TiO_2 is one of the important semiconductor photo-catalysts. A semiconductor photo-catalyst is a wide band gap semiconductor that can increase the rate of certain chemical reactions when exposed to light without directly participating in the reactions. The chemical/photochemical stability of TiO_2 is very high in comparison with other metal oxide materials[10]. It can be easily prepared and analysed by several experimental techniques thereby making it a preferred system for experimentalists [6].

Anatase is an auspicious material for Thin-Film solar panels except for its wide band gap which restrict it to utilize only about 4% of the solar energy[11]. The efficiency of monocrystalline is

between 15-20% and polycrystalline between 13-16%. Thin-film solar panel prototypes have efficiencies range of 7–13% while production modules have efficiency of about 9% subject to manufacturing techniques. Future module efficiencies are anticipated to range between 10% and 16% [12]. Interest in thin-film solar panels was driven by the relevant advantages it offers like simple mass-production technique thereby dropping the price of solar panels drastically, it can be made flexible giving way to new potential applications. Temperature variation has less impact on its performance and it can be used where there is restriction in space.

In order to improve anatase efficiency for solar application, band gap narrowing has been suggested as a way for the material to absorb major part of the solar spectrum [11]. Doping has been reported as a potential means of band narrowing for TiO_2 [13]. Doping is the addition of impurities to in order to produce or modify the properties of a material. Doping anatase with Nitrogen (N) atom had been reported to improve optical absorption in the visible light region [14] due to band narrowing introduced by the dopant. However there is controversy on the source of the phenomenon responsible for band narrowing; it has been reported that band narrowing of anatase was due to mixing of the valence band with Nitrogen 2p states [15]; experimentalists reported that it was due to localized Nitrogen 2p states[14, 16] while other theoretical studies also concluded it was due to localized gap Nitrogen 2p states above the Valence band Maximum (VBM) because mixing of Nitrogen 2p and Oxygen 2p was considered too weak to yield substantial band narrowing[17, 18].

Optical properties of material refer to the response of such materials when exposed to electromagnetic radiation. Optical properties of materials are crucial and over the years it has been extensively investigated for several materials with promising applications. In order to investigate the optical properties of a material, it is necessary to study the complex dielectric function, $\epsilon(\omega)$ which is defined as [19]

$$\epsilon(\omega) = \epsilon_1(\omega) + i \epsilon_2(\omega) \tag{1}$$

where $\epsilon_1(\omega)$ is the real part and $\epsilon_2(\omega)$ is the imaginary part of dielectric function, which is mainly related to the electronic structure of a compound. Other optical constants, such as the refractive index $n(\omega)$, extinction coefficient $k(\omega)$, optical reflectivity $R(\omega)$, absorption coefficient $\alpha(\omega)$, energy-loss spectrum $L(\omega)$, and complex conductivity function $\sigma(\omega)$, can be gained from the complex dielectric function $\epsilon(\omega)$. The imaginary part of dielectric function describes electronic absorption of materials while the real part relates to the electronic polarizability of materials. The real part of the complex dielectric function $\epsilon_1(\omega)$ can also be evaluated from the imaginary part $\epsilon_2(\omega)$ through the famous Kramer's Kronig relationship [19]. The imaginary part of the dielectric constant $\epsilon_2(\omega)$ can be described as [20, 21]

$$\epsilon_2(\hbar\omega) = \frac{2e^2\pi}{\Omega\epsilon_0} \sum_{c,v} \sum_k \left| \langle \psi_k^c | \hat{u}.r | \psi_k^v \rangle \right|^2 \delta(E_k^c - E_k^v - \hbar\omega) \tag{2}$$

where Ω is the volume of the elementary cell, vector u represents the polarization direction of the electric field of the incident photon, v represents the valence band while c represents the

conduction band, k represents the reciprocal lattice vector, and ω represents the frequency of the incident photon while \hbar represents the normalised Planck constant. $\langle \psi_k^c | \hat{u}.r | \psi_k^v \rangle$ represents the matrix elements that determine the probabilities of excitations of electrons occurring from the energy levels in the valence band (E_k^v) to the energy levels in the conduction band (E_k^c) i.e. inter-band transitions.

Equation 1 shows the relationship between the dielectric function, $\epsilon(\omega)$ and imaginary part of dielectric function $\epsilon_2(\omega)$ while equation 2 shows the relationship that exists between the imaginary part of dielectric function $\epsilon_2(\omega)$ and electronic band structure. Optical transition peaks correspond to optical transitions between two states while the intensity of peaks is proportional to density of states.

The valence electronic configurations of the pseudopotentials are $2s^22p^4$ for oxygen, $2s^22p^3$ for nitrogen and $3s^23p^63d^24s^2$ for titanium because only the outer shell electrons are considered. Inner shell electrons are often localized around its ion and do not contribute to covalent bonds. So, instead of a physical potential for the nucleus and the inner electrons, a pseudopotential is used that simulates the effects of a nucleus potential that is screened by its inner electrons. The 2x2x1 supercell of pure anatase TiO_2 consists of 48 atoms (i.e. 16 Titanium atoms and 32 Oxygen atoms). For the N doped anatase one out of the 32 oxygen atoms was replaced with one Nitrogen atom which

corresponds to 3.1% impurity level of doping.

Computational Methodology

Anatase is a tetragonal structure with space group number 141 (space group D_{4h}^{19} -I4₁/amd with Patterson symmetry I4/mmm) containing four titanium (cations) and eight oxygen

(anions) atoms [22]. The titanium atoms are located at the Wyckoff positions 8(c) while the oxygen atoms occupied the 16(f) Wyckoff positions as highlighted in table of Wyckoff position for space group 141 in Table 1 respectively, the internal parameter, x of 0.208 was used[23].

Table 1: The Wyckoff positions of the group 141 (I4₁/amd)[23]

Atom	Multiplicity	Wyckoff letter	Site symmetry	Coordinates
O	16	f	.2.	(x,0,0) (-x+1/2,0,1/2) (1/4,x+3/4,1/4) (1/4,-x+1/4,3/4) (-x,0,0) (x+1/2,0,1/2) (3/4,-x+1/4,3/4) (3/4,x+3/4,1/4)
Ti	8	c	.2/m.	(0,0,0) (1/2,0,1/2) (1/4,3/4,1/4) (1/4,1/4,3/4)

The atomic positions for bulk anatase was generated based on the Wyckoff positions 8(c) for Ti atoms and 16(f) for Oxygen highlighted in Table 1. The generated atomic positions for bulk anatase are:

- Ti 0.000000000 0.000000000 0.000000000
- Ti 0.500000000 0.000000000 0.500000000
- Ti 0.250000000 0.750000000 0.250000000
- Ti 0.250000000 0.250000000 0.750000000
- O 0.208000000 0.000000000 0.000000000
- O 0.292000000 0.000000000 0.500000000
- O 0.250000000 0.958000000 0.250000000
- O 0.250000000 0.042000000 0.750000000
- O -0.208000000 0.000000000 0.000000000
- O 0.458000000 0.000000000 0.500000000
- O 0.750000000 0.042000000 0.750000000
- O 0.750000000 0.958000000 0.250000000

The structures of anatase are shown in Fig. 1 for primitive unit cell, pure 2x2x1 supercell and N-doped 2x2x1 supercell with label A, B and C respectively. The Brillouin zone integration was done using the Monkhorst-Pack set of k-points[24]. Tetrahedron method was used for density of states (DOS)

calculation with Blöchl corrections for precision [25]. The geometry of anatase TiO₂ bulk parameters was optimised using Broyden-Fletcher-Goldfarb-Shanno (BFGS) scheme [26]at different sets of k-points and energy cutoff to evaluate their effects on the bulk parameters. In order to dope(introduce a

moderate impurity to alter electronic and optical properties) anatase TiO_2 with Nitrogen (N), we created a $2 \times 2 \times 1$ supercell from the bulk anatase as shown in fig 1(B), thereafter; one oxygen atom was substituted with a Nitrogen atom as shown in fig 1(C). The $2 \times 2 \times 1$ N-doped anatase TiO_2 is made up of 16 Ti atoms, 31 oxygen atoms and 1 Nitrogen atom ($\text{T}_{16}\text{O}_{31}\text{N}_1$) which gives an impurity level of 3.1% concentration. Guo et al[27] stated that anatase TiO_2 doped with metal usually suffers from thermal instability and electronic states of cationic dopant may serve as carrier recombination centers leading to the photo-catalytic ability being decreased thus we decided to doped anatase with Nitrogen which is a non-metal. To account for the strongly correlated interactions of the Ti d electrons (i.e. d-

d Coulomb interaction in the titanium atoms), a moderate on-site Coulomb Repulsion $U=12.5\text{eV}$ was applied to the calculation of electronic structures so as to obtain a more accurate electronic band gap comparable to experimental value of 3.20eV [28]. The choice of U was made after a series of calculations with different Coulomb interaction parameters, U .

The optical properties calculations for pure and doped anatase were performed within the Density Functional Theory (DFT) as implemented in quantum espresso code[29] to investigate their ground state properties. The ground state properties are then post-processed by Linear Response Theory according to the Bethe-Salpeter-Equation (BSE[30]) as implemented in YAMBO code[31].

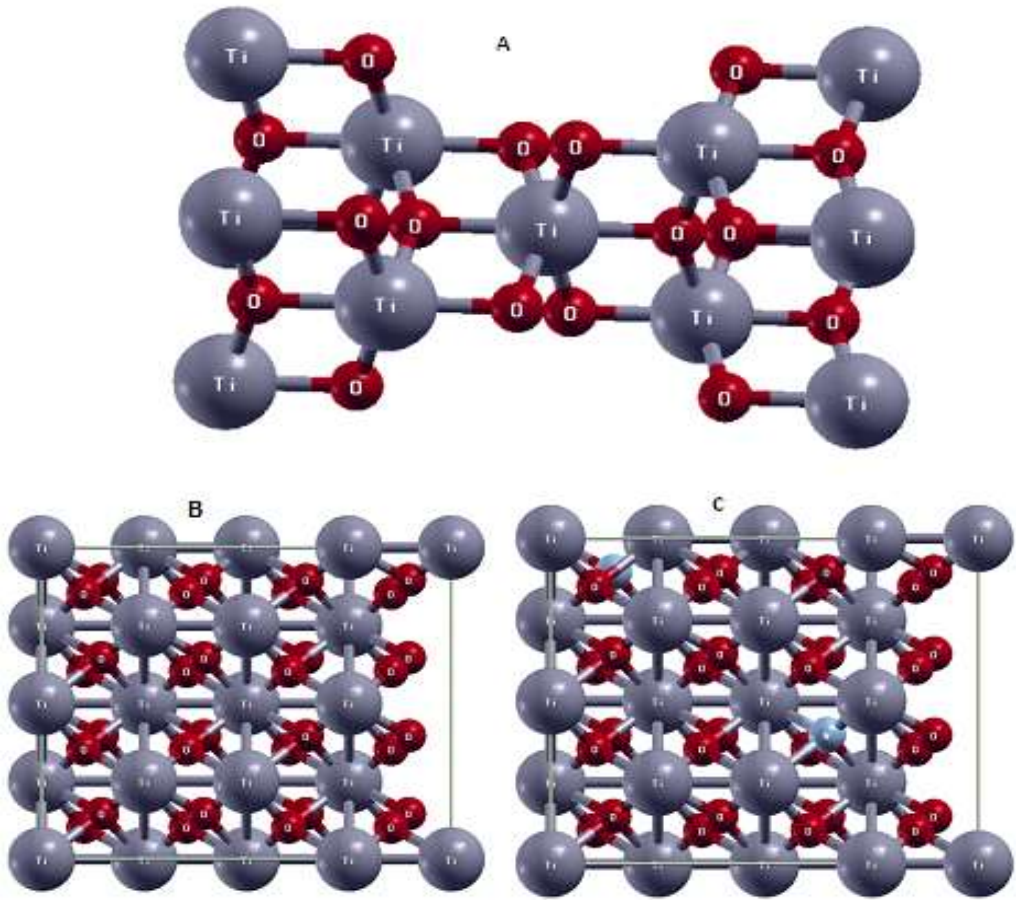


Fig. 1: (A) The tetragonal unit cell of Anatase Structure. (B) Pure Anatase 221 Supercell. (C) is 3.1% N-Doped Anatase 221 Supercell(Drawn using xcrystden[32])

Results and Discussion

Electronic Properties

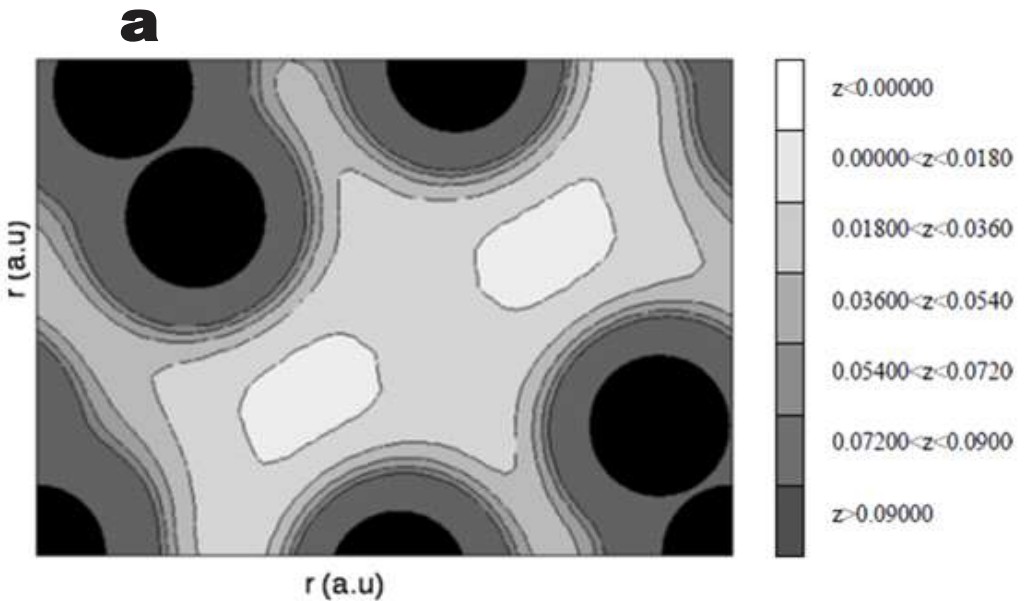
The 2D-cut of the charge density map for Anatase TiO₂ and the electron density map for Anatase TiO₂ along (100) plane are shown in figure 2. The band structure calculation for anatase followed the high symmetry points of the Brillouin Zone for Body Centred Tetragonal (BCT1) system as shown in figure 3(a) from where we adopted the high symmetry direction of Z – Γ – X –

P – N – Γ shown in figure 3(b). The calculated band structures for anatase TiO₂ within the local density approximation (LDA) with exchange correlation functional PZ (Perdew and Zunger) [33] and CP (Cole and Perdew) [34] gave indirect band gap of approximately 2.20eV (i.e. 2.21eV and 2.18eV respectively), obtained between X and P points for both functional. For the exchange correlation functional of Becke –Lee – Yang – Parr, BLYP [35,

36] and Perdew – Burke – Ernzerhof, PBE [37], indirect band gap of 2.36eV was obtained between X and P points. Results for band gaps (2.21eV, 2.18eV and 2.36eV) obtained for both LDA and GGA calculations compares favorably with available theoretical calculations results [38-40] as shown in Table 2. However, they are all considered to underestimate the band gap with respect to the experimental result of 3.2eV [28]. This underestimation of band gaps can be attributed to the choice of exchange correlation functional as can be seen from the results where different functionals gave different electronic

band gaps which is a general deficiency attributed to density functional theory (DFT). The accuracy of DFT calculation is directly related to the accuracy of the functional used.

Fig. 4 shows the Electronic Band Structure of pure Anatase along the high symmetry directions of the Brillouin zone within framework of the GGA + U approach. The calculation was done with Exchange-correlation functional of Becke-Lee-Yang-Parr, BLYP [35, 36]. The band gap of 3.10eV was obtained which compares better with experimental result of 3.20eV of Burdett et al. [28].



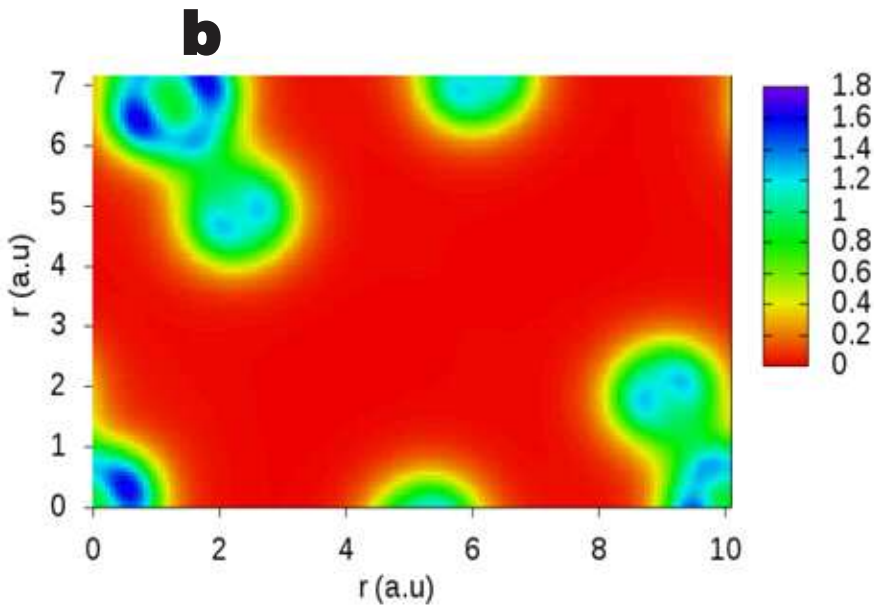


Fig. 2: (a) 2D Cut of the Charge Density of Anatase. (b) Electron Density Map for Anatase

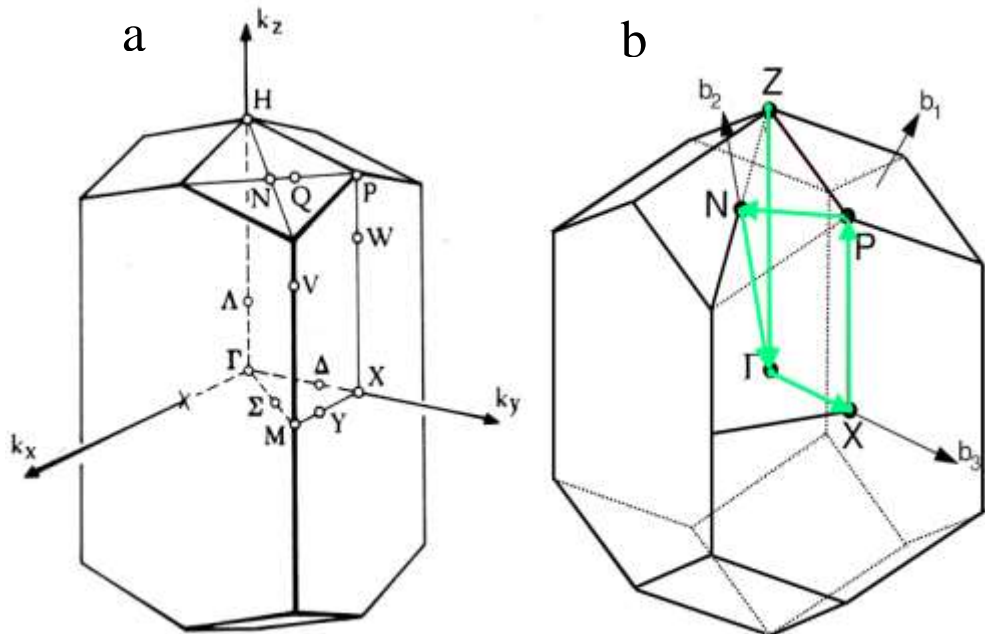
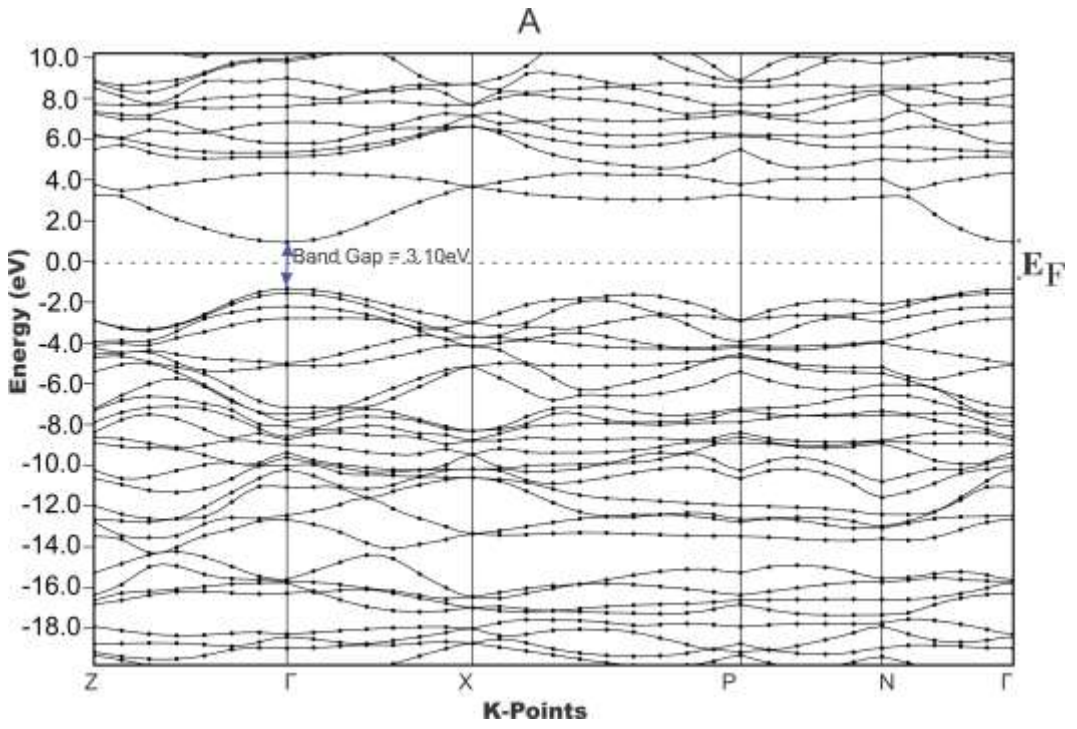


Fig. 3: (a) Brillouin Zone high symmetry points for Body Centred Tetragonal system (b) High Symmetry points direction for Anatase Band Structure Calculation (Points generated with xcrystden)

URL: <http://journals.covenantuniversity.edu.ng/index.php/cjpls>

Table 2: Comparison of four calculated band gap and lattice parameters for anatase TiO₂ with available theoretical and experimental results

BandGapE _g (eV)	Lattice Parameter		Potential	Code / Method	Reference
	a (Å)	c (Å)			
Theoretical Results					
2.18 ¹ , 2.21 ¹	3.8182	9.6871	LDA-DFT	Quantum Espresso	This Work
2.36 ¹ 2.39 ¹ 3.10	3.7121 3.7751 3.7751	9.5802 9.5116 9.5116	GGA-DFT BLYP GGA-DFT PBE GGA-DFT+U(12.5eV) PBE		
2.15 ¹ , 2.43 3.83 ¹ , 4.29	3.81	9.64	GGA-DFT PBE GoWo		
2.34	3.801	9.778	PBE-GGA	CASTEP	[41]
2.679	-	-	mBJ FPAPW	WIEN2K	[42]
2.8 ¹	3.832	9.599	GGA+U	VASP	[43]
2.11 2.295	3.829	9.702	GGA-DFT GGA+U	CASTEP	[44]
2.13	3.80	9.67	GGA-DFT PBE	CASTEP	[45]
2.3	-	-	LAPW	WIEN2K	[46]
2.811	3.7973	9.7851	GGA PW91	CASTEP	[47]
2.12	3.784	9.515	DFT	CASTEP	[48]
2.14 ¹ 2.89 ¹	-	-	GGA-DFT GGA-DFT+U (6.6eV)	CASTEP	[49]
2.0	3.77	9.46	FP-LAPW	VASP	[50]
Experimental Results					
			Method		
3.20	3.785	9.502	Pulsed Neutron Diffraction		[28]
3.3	3.784	9.515	Absorption Photodesorption of Oxygen		[51]



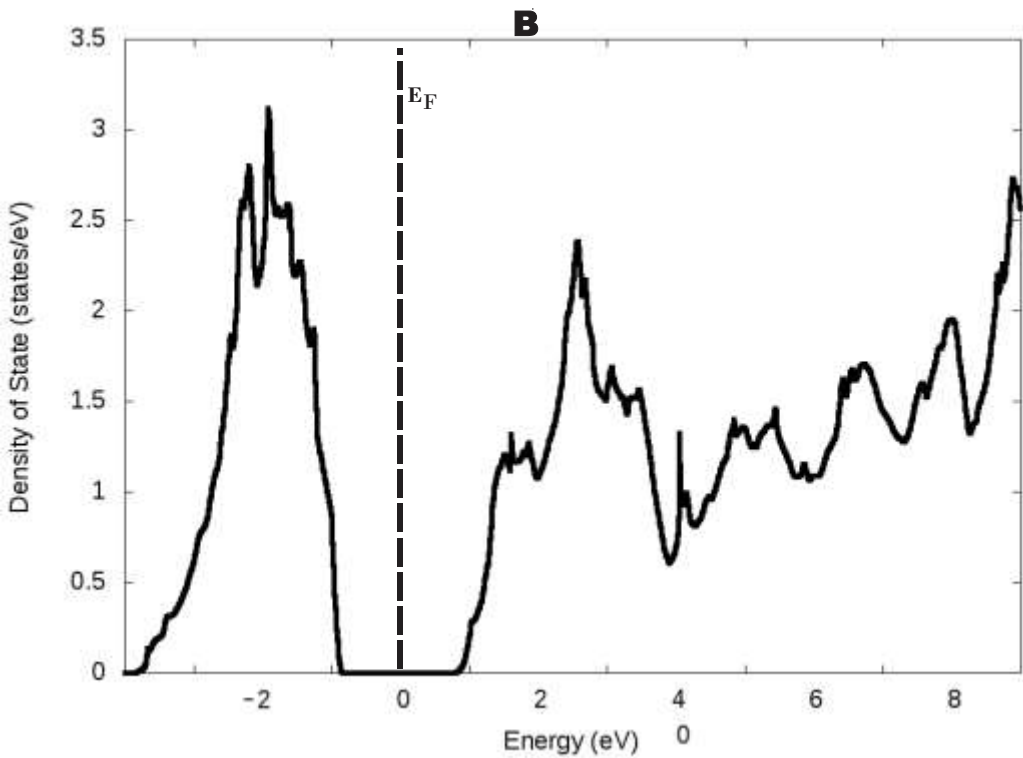


Fig. 4: (A) is the Band Structure of Pure Anatase for GGA+U Calculation. (B) is DOS from A.

The Partial density of states (PDOS) for all states in anatase TiO_2 shows that the valence band maximum (VBM) of pure anatase TiO_2 predominantly consists of the O 2p states while the conduction band minimum (CBM) is predominantly of Ti d states, however, the hybridization between the Ti d and O 2p levels at the valence band can be observed. PDOS reveals the bands of electronic band structure with respect to their electronic states and contribution to the band gap. The lowest part of the valence bands are predominantly made up of O - 2(s) states with little mixture of the Ti - p and Ti - s states.

The band structure for the N-doped anatase is shown in Fig. 5 with a direct band gap of 1.47 eV at Γ point. There was a shift in the Fermi level of the N-doped anatase band structure towards the conduction band, which may be due to charge balance between the dopant and the host lattice. This shift in the Fermi level thereby contributes to the reduction in the band gap as also reported by [45] for their Ag (Silver) doped anatase. PDOS shows that the valence bands consist mainly of the O 2p states within the energy range of -4.0 eV and 0 eV while the conduction band is predominantly Ti 3d states within the energy range of 0 eV and 6.0 eV. The

extra band between VBM and CBM can be seen to come from the N 2p states as a result of the Nitrogen dopant. It can be

inferred that nitrogen impurity atom (dopant) was able to modify the electronic structure of anatase.

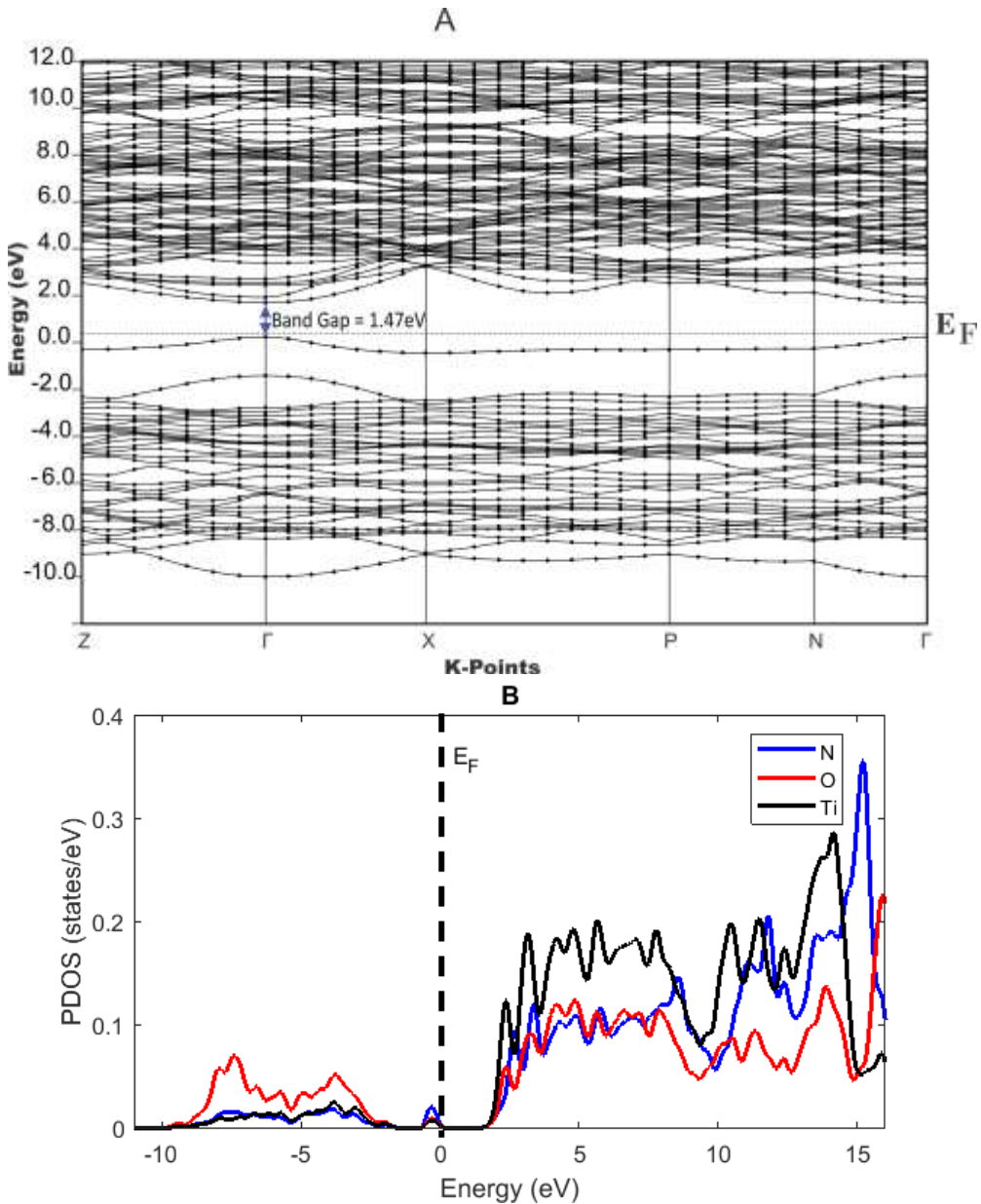


Fig. 5: A is Band Structure of 3.1% N-Doped Anatase ($Ti_{16}O_{31}N_1$). B is the Calculated PDOS for A.

URL: <http://journals.covenantuniversity.edu.ng/index.php/cjpls>

Optical Properties

Figure 6 shows the comparison of the imaginary part of the frequency dependent dielectric spectrum for pure and N-doped anatase TiO₂. The comparison of the real part of the dielectric spectrum for pure and N-doped anatase TiO₂ indicate six different optical peaks for doped specie at D1 to D6 with respective energy values of 0.5eV, 0.7eV, 1.2eV, 1.8eV, 2.3eV and 3.5eV. The result obtained by [49]for N-doped anatase shows two peaks at about 1.8eV and 4.22eV. For the pure anatase with increase of energy response, 5.5eV optical transition can be observed, which indicate optical response of the imaginary part of the dielectric function for band gap. After doping with nitrogen, N the optical transition from band gap decreases to 3.5eV. This shift of the optical transition indicates that the band gap of the doped anatase was reduced as described in our result for the band structure and density of states

(DOS). The highest peak transition was observed at 0.7eV in the low energy region which can lead to the shift of valence band to dopant states.

The intrinsic anatase shows the optical absorption peaks at the ultraviolet (UV) region of the electromagnetic spectrum while the N-doped anatase has optical absorption peaks in the visible light region. N-doped anatase shows a wider range of optical absorption peaks than N-doped rutile which may be due to presence of a more distinct band between the Valence Band Minimum (VBM) and Conduction Band Maximum (CBM). This band between the VBM and CBM comes from the contribution of N 2p states as seen earlier in the partial density of states (PDOS) for N-doped anatase. These widely distributed optical peaks may be able to increase the absorption of photons in the visible light region of the electromagnetic spectrum.

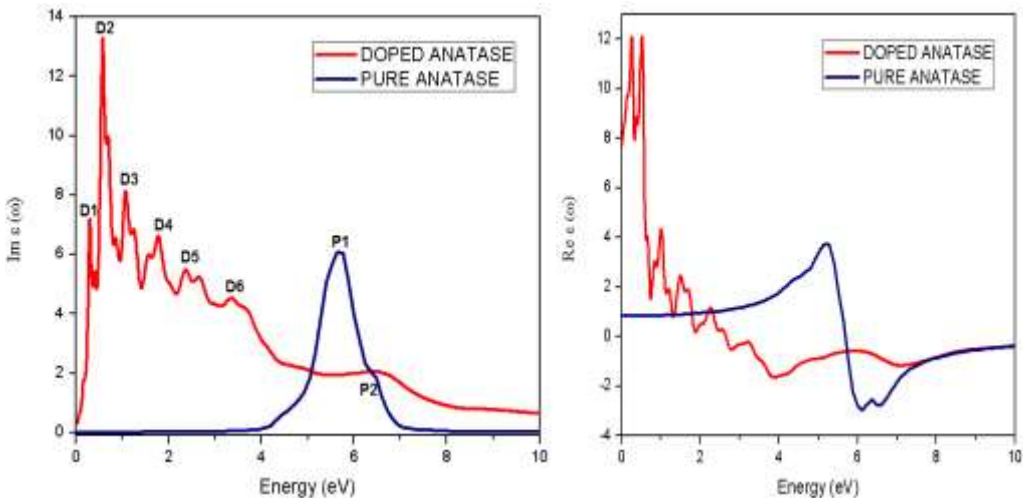


Fig. 6: Comparison of Imaginary part and real part of the frequency dependent dielectric function of Pure Anatase and 3.1% Concentration N-Doped Anatase respectively.

Conclusion

In this work, the electronic and optical properties of body centered tetragonal TiO₂ anatase (pure and doped) have been carried out within the density functional theory in the local density approximation (LDA) and the generalized gradient approximation (GGA) with the inclusion of Coulomb interaction parameter, U. The energy band gap, the density of states, partial density of states and frequency dependent dielectric functions were calculated. Pure anatase have their Fermi level located in the gap showing insulating properties. Doping with one

Nitrogen atom resulted in the upward shift of Fermi level towards the conduction band thereby reducing the band gap. From the optical properties of N-doped anatase analysis, N-doped anatase may be a good base material for photovoltaic application because of the optical peaks exhibited in the visible light region of electromagnetic spectrum.

Acknowledgement

Olayinka A.S. wishes to thank Forschungszentrum Julich, Germany and ICTP (Ref: 23100000) for the respective supports in the course of this research.

References

respective supports

- [1] Debut B. (2016) South Africa Basks in Continent's First Solar-Powered Airport. <http://phys.org/news/2016-10-south-africa-basks-continent-solar-powered.html>;
- [2] Ajayi O.O., Ohijeagbon, O.D, Nwadialo, C.E. and Olasope, O. (2014). New Model to Estimate Daily Global Solar Radiation over Nigeria. *Sus. Energy Tech. & Ass.* 5, 28-36.
- [3] Long R., English N.J. (2010). Electronic Properties of F/Zr Co-Doped Anatase TiO₂ Photocatalysts from GGA+ U Calculations. *Chem. Phys. Lett.* 498, 338-44.
- [4] O'Regan B., Grätzel M. (1991). A Low-Cost, High-Efficiency Solar Cell Based on Dye-Sensitized Colloidal TiO₂ Films. *Nature* 353. 737.
- [5] Devi L.G., Murthy B.N., Kumar S.G. (2009). Photocatalytic Activity of V⁵⁺, Mo⁶⁺ and Th⁴⁺ Doped Polycrystalline TiO₂ for the Degradation of Chlorpyrifos under UV/Solar Light. *J. of mol. catal A: Chem.* 308, 174-81.
- [6] Diebold U. (2003). The Surface Science of Titanium Dioxide. *Surf. Sc. Reports* 48, 53-229.
- [7] Olayinka, A. S., Adetunji, B. I., Idiodi, J. O. A. and Aghemelon U. (2019). Ab initio study of electronic and optical properties of nitrogen-doped rutile TiO₂. *Int. J. of Mod. Phys. B.* 33(06), 1950036
- [8] Diebold U. (2003). Structure and Properties of TiO₂ Surfaces: A Brief Review. *App. Phys. A* 76, 681-7.
- [9] Gong X.-Q., Selloni A., Vittadini A. (2006). Density Functional Theory Study of Formic Acid Adsorption on Anatase TiO₂ (001): Geometries, Energetics, and Effects of Coverage, Hydration, and Reconstruction. *The J. of Phy Chem. B* 110, 2804-11.
- [10] De Lasa H., Serrano B. and Salices M., (2005) Photocatalytic Reaction Engineering. Springer Science,

- Business Media Inc., Spring Street, New York, NY10013.
- [11] Han X. and Shao G. (2011). Electronic Properties of Rutile TiO₂ with Nonmetal Dopants from First Principles. *The J. of Phy. Chem. C* **115**, 8274-82.
- [12] Maehlum M.A. (2015). Which Solar Panel Type Is Best? Mono- Vs. Polycrystalline Vs. Thin Film. <http://www.energyinformative.org/best-solar-panel-monocrystalline-polycrystalline-thin-film/> 2015.
- [13] Mi L., Xu P., Shen H., Wang P. N., and Shen W. (2007). First-Principles Calculation of N: H Codoping Effect on Energy Gap Narrowing of TiO₂. *App. Phy. Lett.* **90**, 171909.
- [14] Irie H., Watanabe Y., Hashimoto K. (2003). Nitrogen-Concentration Dependence on Photocatalytic Activity of TiO₂-X N X Powders. *The J. of Phy. Chem. B* **107**, 5483-6.
- [15] Asahi R., Morikawa T., Ohwaki T., Aoki K., Taga Y. (2001). Visible-Light Photocatalysis in Nitrogen-Doped Titanium Oxides. *Science* **293**, 269-71.
- [16] Lindgren T., Mwabora J., Avendano E., Jonsson J., Hoel A., Granqvist C. G and Lindquist S. E. (2003). Photoelectrochemical and Optical Properties of Nitrogen Doped Titanium Dioxide Films Prepared by Reactive DC Magnetron Sputtering. *J. Phys Chem B*.**107(24)**, 5709-5716.
- [17] Lee J.-Y., Park J., and Cho J.-H. (2005). Electronic Properties of N-and C-Doped TiO₂. *App. Phy. Lett.* **87**, 011904.
- [18] Long M., Cai W., Wang Z., and Liu G. (2006). Correlation of Electronic Structures and Crystal Structures with Photocatalytic Properties of Undoped, N-Doped and I-Doped TiO₂. *Chem. Phy. Lett.* **420**, 71-6.
- [19] Ambrosch-Draxl C., and Sofo J.O. (2006). Linear Optical Properties of Solids within the Full-Potential Linearized Augmented Planewave Method. *Comp. Phy. Comm.* **175**, 1-14.
- [20] Ibach H., and Lüth H. (2009) *Dielectric Properties of Materials. Solid-State Physics: Springer*, p. 371-418.
- [21] Wooten F. (1972). *Optical Properties of Solids, Academic, New York.*
- [22] Tilley R. (2006). *Crystal and Crystal Structures: John Wiley & Sons Ltd, West Sussex, England.*;
- [23] Aroyo M.I., Perez-Mato J.M., Capillas C., Kroumova E., Ivantchev S., Madariaga G., Kirov A. and Wondratschek H. . (2006). Bilbao Crystallographic Server I: Databases and Crystallographic Computing Programs. *Z Krist* **221**, 1527.
- [24] Monkhorst H.J., Pack J.D. (1976). Special Points for Brillouin-Zone Integrations. *Phy. Rev. B* **13**, 5188.
- [25] Blöchl P.E., and Jepsen O., Andersen O.K. (1994).

- Improved Tetrahedron Method for Brillouin-Zone Integrations. *Phy. Rev. B* **49**, 16223.
- [26] Fischer T.H., and Almlof J. (1992). General Methods for Geometry and Wave Function Optimization. *The J.of Phy. Chem.* **96**, 9768-74.
- [27] Guo W., Wu L., Chen Z., Boschloo G., Hagfeldt A., and Ma T. (2011). Highly Efficient Dye-Sensitized Solar Cells Based on Nitrogen-Doped Titania with Excellent Stability. *J. of Photochem.and Photobio. A: Chem.* **219**, 180-7.
- [28] Burdett J.K., Hughbanks T., Miller G.J., Richardson Jr J.W., and Smith J.V. (1987). Structural-Electronic Relationships in Inorganic Solids: Powder Neutron Diffraction Studies of the Rutile and Anatase Polymorphs of Titanium Dioxide at 15 and 295 K. *J. of the American Chem. Soc.* **109**, 3639-46.
- [29] Giannozzi P., Baroni S., Bonini N., Calandra M., Car, R., Cavazzoni C., Ceresoli D., Chiarotti G. L., Cococcioni M., Dabo I., Dal Corso A., Fabris S., Fratesi, G., de Gironcoli S., Gebauer R., Gerstmann U., Gougoussis C., Kokalj A., Lazzeri M., Martin-Samos L., Marzari N., Mauri F., Mazzarello R., Paolini S., Pasquarello A., Paulatto L., Sbraccia C., Scandolo S., Sclauzero G., Seitsonen A. P., Smogunov A., Umari P. and Wentzcovitch R. M. (2009). QUANTUM ESPRESSO: a modular and open-source software project for quantum simulations of materials. *J. Phys.: Condens. Matter* **21**, 395
- [30] Salpeter E.E., and Bethe H.A. (1951). A Relativistic Equation for Bound-State Problems. *Phy.Rev.* **84**, 1232.
- [31] Marini A., Hogan C., Grüning M., and Varsano D. (2009). Yambo: An Ab Initio Tool for Excited State Calculations. *Comp. Phy. Comm.* **180**, 1392-403.
- [32] Kokalj A. (2003). Computer Graphics and Graphical User Interfaces as Tools in Simulations of Matter at the Atomic Scale. *Comp. Mat. Sc.* **28**, 155-68.
- [33] Perdew J.P., and Zunger A. (1981). Self-Interaction Correction to Density-Functional Approximations for Many-Electron Systems. *Phy. Rev. B* **23**, 5048.
- [34] Cole L.A., and Perdew J. (1982). Calculated Electron Affinities of the Elements. *Phy. Rev. A* **25**:1265.
- [35] Becke A.D. (1988). Density-Functional Exchange-Energy Approximation with Correct Asymptotic Behavior. *Phy.Rev. A* **38**, 3098.
- [36] Lee C., Yang W., and Parr R.G. (1988). Development of the Colle-Salvetti Correlation-Energy Formula into a Functional of the Electron Density. *Phy. Rev. B* **37**, 785.
- [37] Perdew J.P., Burke K., and Ernzerhof M. (1996).

- Generalized Gradient Approximation Made Simple. *Phys. Rev. Lett.* **77**, 3865.
- [38] Chiodo L., García-Lastra J.M., Iacomino A., Ossicini S., Zhao J., Petek H. (2010). Self-Energy and Excitonic Effects in the Electronic and Optical Properties of TiO₂ Crystalline Phases. *Phys. Rev. B* **82**, 045207.
- [39] Labat F., Baranek P., Domain C., Minot C., and Adamo C. (2007). Density Functional Theory Analysis of the Structural and Electronic Properties of TiO₂ Rutile and Anatase Polytypes: Performances of Different Exchange-Correlation Functionals. *The J. of Chem. Phys.* **126**, 154703.
- [40] Yang K., Dai Y., Huang B. (2007). Understanding Photocatalytic Activity of S- and P-Doped TiO₂ under Visible Light from First-Principles. *The J. of Phys. Chem. C* **111**,:18985-94.
- [41] Li N., Yao K., Li L., Sun Z., Gao G., and Zhu L. (2011). Effect of Carbon/Hydrogen Species Incorporation on Electronic Structure of Anatase-TiO₂. *J. of App. Phys.* **110**, 073513.
- [42] McLeod J., Green R., Kurmaev E., Kumada N., Belik A., and Moewes A. (2012). Band-Gap Engineering in TiO₂-Based Ternary Oxides. *Phys. Rev. B* **85**, 195201.
- [43] Zhang Y.G., Wang Y.X. (2011). Calculations Show Improved Photoelectrochemical Performance for N, Ce, and Ce+ N Doped Anatase TiO₂. *J. of Applied Physics* **110**, 033519.
- [44] Khan M., Xu J., Chen N., and Cao W. (2012). Electronic and Optical Properties of Pure and Mo Doped Anatase TiO₂ Using GGA and GGA+U Calculations. *Physica B: Cond Matter* **407**, 3610-6.
- [45] Khan M., Xu J., Chen N., Cao W., Usman Z., and Khan D. (2013). Effect of Ag Doping Concentration on the Electronic and Optical Properties of Anatase TiO₂: A DFT-Based Theoretical Study. *Research on Chem Intermediates* **39**, 1633-44.
- [46] Zhang R., Wang Q., Li Q., Dai J., and Huang D. (2011). First-Principle Calculations on Optical Properties of C-N-Doped and C-N-Codoped Anatase TiO₂. *Physica B: Cond. Matt.* **406**, 3417-22.
- [47] Zhang R., Wang Q., Liang J., Li Q., Dai J., Li W. (2012). Optical Properties of N and Transition Metal R (R= V, Cr, Mn, Fe, Co, Ni, Cu, and Zn) Codoped Anatase TiO₂. *Physica B: Cond. Matt.* **407**, 2709-15.
- [48] Liu X., Jiang E., Li Z., and Song Q. (2008). Electronic Structure and Optical Properties of Nb-Doped Anatase TiO₂. *App Phys. Lett.* **92**, 252104.
- [49] Guo M., and Du J. (2013). Electronic and Optical Properties of C-N-Codoped TiO₂, A First-Principles GGA+U Investigation. *Inter J. of Modern Phys. B* **27**, 1350123.

[50] Lei Y., Liu H., and Xiao W. (2010). First Principles Study of the Size Effect of TiO₂ Anatase Nanoparticles in Dye-Sensitized Solar Cell. Modelling and Simulation in Materials Science and Engineering **18**, 025004.

[51] Linsebigler A.L., Lu G., and Yates Jr J.T. (1995). Photocatalysis on TiO₂ Surfaces: Principles, Mechanisms, and Selected Results. Chem. Rev 95:735-58.